



Two Practical Methods to Retrieve Aerosol Optical Properties from Coherent Doppler Lidar

Yinchao Zhang, Yize Zheng, Wangshu Tan * , Pan Guo, Qingyue Xu, Su Chen, Ruiqi Lin, Siying Chen and He Chen

School of Optics and Photonics, Beijing Institute of Technology, Beijing 100081, China; ychang@bit.edu.cn (Y.Z.); 3220190453@bit.edu.cn (Y.Z.); guopan@bit.edu.cn (P.G.); xu_qingyue@bit.edu.cn (Q.X.); su_chen@bit.edu.cn (S.C.); 3120190549@bit.edu.cn (R.L.); csy@bit.edu.cn (S.C.); shinanshao@bit.edu.cn (H.C.)

* Correspondence: tanws@bit.edu.cn

Abstract: Complexly distributed aerosol particles have significant impacts on climate and environmental changes. As one of the vital atmospheric power sources, the wind field deeply affects the distribution and transport of aerosol particles. For a more comprehensive investigation of the aerosols flux and transport mechanism, two retrieval methods of aerosol optical properties (backscatter coefficient and extinction coefficient at 1550 nm) from coherent Doppler lidar (CDL) observation are proposed in this paper. The first method utilizes the calculated aerosol backscatter coefficient (532 nm) from Mie-scattering lidar datasets and the iterative Fernald method to retrieve aerosol optical property profiles during joint measurements with CDL and Mie-scattering lidar. After verifying the correctness of the first method compared with AERONET datasets, we proposed the second retrieval method. Using the forward integral Fernald method with near-ground reference aerosol extinction coefficient calculated by atmospheric visibility, aerosol optical properties at 1550 nm could be obtained. Thirty-six-day joint measurements with two lidars were specially designed and conducted to verify the correctness of these retrieval methods. The validation results of these two methods indicate great performances, where the mean relative errors are 0.0272 and 0.1656, and the correlation coefficients are 0.9306 and 0.9197, respectively. In conclusion, the feasibility of these two retrieval methods extends the capability of CDL to detect aerosol optical properties and also provides a possibility to observe the aerosol distribution and transport process comprehensively, which is a great promotion of aerosol transport studies development.

Keywords: coherent doppler lidar; aerosol optical properties; Mie-scattering lidar; atmospheric visibility



Citation: Zhang, Y.; Zheng, Y.; Tan, W.; Guo, P.; Xu, Q.; Chen, S.; Lin, R.; Chen, S.; Chen, H. Two Practical Methods to Retrieve Aerosol Optical Properties from Coherent Doppler Lidar. *Remote Sens.* **2022**, *14*, 2700. <https://doi.org/10.3390/rs14112700>

Academic Editor: Michaël Sicard

Received: 25 April 2022

Accepted: 2 June 2022

Published: 4 June 2022

Publisher's Note: MDPI stays neutral with regard to jurisdictional claims in published maps and institutional affiliations.



Copyright: © 2022 by the authors. Licensee MDPI, Basel, Switzerland. This article is an open access article distributed under the terms and conditions of the Creative Commons Attribution (CC BY) license (<https://creativecommons.org/licenses/by/4.0/>).

1. Introduction

As a vital constituent of the atmosphere, aerosols are mainly distributed in the planetary boundary layer (PBL), regarded as the interface between the free atmosphere and Earth's surface. The aerosol vertical transport and interaction with solar radiation in the PBL significantly influence the weather and climate [1]. Estimating and evaluating such a mechanism is challenging, due to the spatiotemporal variability of aerosol particle amounts and properties. Hence, vertically resolved measurements of aerosol optical properties and transport processes have attracted lots of interest [2].

The study of aerosols' temporal and spatial variation is inseparable from the support of remote sensing techniques. Benefitting from the development of modern laser remote sensing technology, as one of the important atmospheric science research methods, lidar has become a reliable type of instrument for measuring atmospheric aerosol movement. Meanwhile, aerosol transport is closely related to the changes in wind fields. To comprehensively explore the distribution and long-term transmission of aerosol particles, CDL as a typical wind field detection instrument has been introduced to complete the measurements of aerosol transport processes. The CDL usually provides vector wind fields by detecting

the Doppler shift of the backscattered light excited by aerosols, and the received backscatter light intensity can characterize the aerosol concentration as well. In previous research on aerosols with CDL, wind profiles and received backscatter signals were always provided by CDL for only determining transmission direction and the location of the aerosol layer. Wandinger et al., presented the first results of aerosol flux profiles retrieved by the combined datasets of vertical wind profiles and highly resolved aerosol backscatter signals, which were concurrently detected by the CDL of the Max Planck Institute for Meteorology Hamburg (MPI) and the aerosol Raman lidar of the Institute for Tropospheric Research Leipzig (IfT) [3]. Bou Karam et al., reported the dust transport processes in the tropical discontinuity (ITD) region over western Niger during the near-dawn period through the joint detection of an airborne CDL at 10.6 μm and a differential absorption Lidar at 732 nm [4]. Schumann et al., investigated the distribution of volcanic ash plumes over Europe by 2 μm airborne CDL and in situ aerosols and gas tracing devices, CDL mainly provided wind vector and attenuated backscatter signals to determine the transport direction and location of the aerosol layer [5]. Weinzierl et al., determined the upper and lower boundary layers of aerosol relying on suddenly changed backscatter signal intensity obtained from an airborne 2 μm CDL [6]. However, these joint observations with several lidars cause expensive overhead; at the same time, it also introduces analysis errors in detecting aerosol transport by different lidars.

Meanwhile, many studies reported various methods for retrieving aerosol properties from CDL, and most of these methods depend on the return signals from targets with known optical parameters [7,8]. Compared with aerosol lidars, CDL cannot obtain Rayleigh backscatter signals from the stratosphere or upper troposphere to calibrate aerosol measurements [9,10]. The lower sensitivity of CDL to spectrally broad signals [11] also affects the accuracy of retrieved backscatter power. Therefore, the optical properties and transport processes of aerosol cannot be directly retrieved from the backscattered signal of CDL alone. Thus, CDL and other types of reference instruments are frequently used in simultaneous measurements to perform aerosol flux and investigate the aerosol spatiotemporal transport processes [3,12]. Bufton et al., used a multi-wavelength airborne lidar (355 nm and 532 nm), and a 9.5 μm CDL to obtain sea surface returns for calibrating the mean backscattering efficiency, and made a comparison among different backscatter signals of the ocean surface, sand, and beach [7]. Menzies and Tratt described an airborne CO₂ CDL with a hard-target calibration method to obtain the quantitative aerosol backscatter and extinction profiles near 9 μm [8]. These target calibration methods require extremely strict experimental conditions and a high-performance lidar system. For expanding CDL's ability to detect aerosol optical properties, more reasonable approaches had been reported to calibrate and retrieve aerosol optical properties from CDL. Chouza et al., introduced a new method for calibrating and retrieving aerosol backscatter and extinction from an airborne 2 μm CDL. The accuracy rate of measurement results was more than 80%, compared with Portable Lidar Systems (POLIS) and satellite CALIPSO [13]. This method requires aerosol types, vertical distribution, and particle depolarization coefficient input during calculation. Guangyao Dai et al., indicated a retrieval and calibration method for aerosol optical properties detection with CDL and a sun-photometer, where the sun-photometer offers aerosol optical depth (AOD) as the basis for calibration calculation [14]. The two AODs respectively calculated from CDL and a sun-photometer were compared, the correlation coefficient is greater than or equal to 0.96, and the mean relative error is less than or equal to 0.22. It should be emphasized that the result of this method needs further experimental verification, which is limited by the number of experimental datasets.

Combining the above studies, in this paper, we propose two practical methods to retrieve the vertical spatial–temporal transport of aerosols. The first method is based on the joint measurements with 1550 nm CDL and 532 nm Mie-scattering lidar. By using the reference backscatter coefficient at 532 nm and the proposed iterative Fernald method, aerosol optical properties at 1550 nm could be calculated from the spectra of CDL. Two Ångström exponents respectively calculated from these two lidars and AERONET datasets

were compared to validate the feasibility of this method. After confirming the high accuracy of the first method, the second method was proposed with greater practicality. Based on the atmospheric visibility and the results of the first method, the reference extinction coefficient at 1550 nm could be obtained, then the aerosol optical properties at 155 nm can be retrieved from CDL using the Fernald method. Finally, the results of these two methods were compared to verify the feasibility of the second method.

The organization of this paper is as follows. Section 2 introduces the involved experimental instruments and datasets. Two retrieval methods based on Mie-scattering aerosol lidar and real-time visibility are described, respectively, in Section 3. Moreover, the comparisons, analysis, and discussion of the experimental results are presented in Section 4. Section 5 presents a summary of conclusions and describes the outlook of future studies.

2. Instruments and Datasets

2.1. Coherent Wind Lidar

A portable all-fiber CDL system with laser wavelength at 1550 nm, whose operation relies on the heterodyning technique and doppler effect to measure the wind vector, was placed on the campus of Beijing Institute of Technology (39.95°N, 116.32°E) [15]. However, the most crucial difference between the actual experimental CDL system with the initial lidar system is that we removed the wedge mirror and put the lidar in stare mode for detecting vertical aerosol backscatter light; additionally, other system configurations are the same. The detailed specifications of CDL are summarized and listed in Table 1. After retrieving from the range-resolved power spectra and correction (distance correction, pulse energy correction, heterodyne efficiency correction [13]), the retrieved backscatter signal power was normalized for calculation. The retrieval and correction processes are supplied in Appendix A.

Table 1. The detailed specifications of the all-fiber CDL system.

Qualification	Specification
Wavelength (nm)	1550
Pulse energy (μ J)	50
Pulse width (ns)	400 (100, 200, 400, adjustable)
Pulse repetition rate (kHz)	10
The linewidth of laser (kHz)	15
Range resolution (m)	60
Measurement range (m)	100 to boundary layer ¹
Temporal resolution (s)	1
Telescope aperture (mm)	50
Focal length	∞
Beam diameter (mm)	40
Sampling frequency (GHz)	1
Detection mode	Stare mode
Detector mode	Balanced detector
Bandwidth (MHz)	200

¹ The maximum height of the boundary layer is 2000 m under the normal weather condition in Beijing.

2.2. Mie-Scattering Lidar

The Mie-scattering lidar system wavelength at 532 nm was placed in another room on the campus of Beijing Institute of Technology (39.95°N, 116.32°E) with a straight-line distance of 5 m to the CDL system. This lidar system has been repeatedly upgraded [16,17] for obtaining more specific atmospheric information such as aerosol, temperature, cloud, and aerosol-atmospheric boundary layer height (ABLH); the detailed parameters are listed in Table 2. After lidar system factor correction (background noise error correction, electronic noise error correction, and overlap factor correction) and distance correction, the raw backscatter signal was normalized for retrieval.

Table 2. The detailed specifications of the Mie-scattering aerosol lidar system.

Qualification	Specification
Wavelength (nm)	532
Pulse energy (mJ)	180
Pulse repetition rate (Hz)	20
Telescope	Newtonian
Range resolution (m)	2.5
Measurement range (m)	500 to max 10,000
Temporal resolution (s)	60
Telescope diameter (mm)	400
Field of view (mrad)	0.9
Mode	Coaxial
Half-width of detection channel (nm)	1

2.3. AERONET Datasets

As one of the responsible institutions of AERONET, the Chinese Academy of Meteorological Sciences (CAMS) located in Beijing (39.93°N, 116.317°E) is within 1.2 km of both CDL and Mie-scattering aerosol lidar. This AERONET station provides daily aerosol optical depth (AOD) datasets with eight different wavelengths using measurements of a CIMEL sun-photometer [18], and the temporal resolution is about 5 min in most of the measurements period.

The measured AOD is the column-integrated aerosol extinction coefficient. Each type of aerosol particle has corresponding extinction coefficients for different wavelengths of light and, therefore, is AOD. Thus, the Ångström exponent is introduced to characterize the wavelength dependency of AOD, which is generally defined as the slope on the logarithm of AOD to the logarithm of the wavelength. For obtaining experimental reference data, the Ångström exponent between 532 and 1550 nm $AE_{reference}^{532-1550}$ is estimated from daily AOD datasets using a second-order fit [19,20].

2.4. Atmospheric Visibility Datasets

Regarding the visibility-related retrieval method that we proposed in Section 3, atmospheric visibility is regarded as a crucial factor to calibrate and retrieve aerosol optical properties at 1550 nm of CDL. According to the previous introduction, the backscatter coefficient and extinction coefficient of aerosol cannot be obtained from the retrieved backscatter power of CDL without reference calibration. The near-ground aerosol extinction coefficient $\alpha_{near-ground}$ is introduced as the reference to solve this problem, which could be calculated by Equation (1) [21].

$$\alpha_{near-ground} = \frac{3.91}{U} \left(\frac{\lambda}{550} \right)^{-q} \quad (1)$$

where U is the atmospheric visibility in units of km, and the real-time visibility is obtained from the Official website of China Central Meteorological Observatory [22] during the joint measurement period of two lidars, λ is the laser wavelength of CDL in units of nm, q is the correction factor and was determined by experiments as [23,24]:

$$q = \begin{cases} 1.6 & U > 50 \text{ km} \\ 1.3 & 6 \text{ km} < U < 50 \text{ km} \\ 0.585U^{1/3} & U < 6 \text{ km} \end{cases} \quad (2)$$

3. Methodology

It is generally believed that the backscatter coefficient and extinction coefficient are both affected by aerosols and atmospheric molecules. Hence, the aerosol backscatter

coefficient and extinction coefficient can be calculated using the Fernald method [25] which is expressed as:

$$\begin{cases} \beta_a(R) = -\beta_m(R) + \frac{X(R) \exp[2(S_a - S_m) \int_R^{r_0} \beta_m(r') dr']}{\frac{X(r_0)}{\beta_a(r_0) + \beta_m(r_0)} + 2S_a \int_R^{r_0} X(r') \exp[2(S_a - S_m) \int_r^{r_0} \beta_m(r'') dr''] dr'} & R \leq r_0 \\ \beta_a(R) = -\beta_m(R) + \frac{X(R) \exp[-2(S_a - S_m) \int_0^R \beta_m(r') dr']}{\frac{X(r_0)}{\beta_a(r_0) + \beta_m(r_0)} - 2S_a \int_0^R X(r') \exp[-2(S_a - S_m) \int_0^r \beta_m(r'') dr''] dr'} & R > r_0 \end{cases} \quad (3)$$

where R is the detection height, X is the normalized backscatter signal power, the parameters with subscript a are expressed as atmospheric aerosol related, parameters with subscript m are expressed as atmospheric molecular related, $S_a = \alpha_a / \beta_a$ is the ratio of aerosol extinction coefficient to aerosol backscatter coefficient in the normal weather conditions, $S_m = \alpha_m / \beta_m = 8\pi/3$ is the ratio of molecular extinction coefficient to molecular backscatter coefficient, r_0 is the reference height usually higher than 6 km. Noteworthy, S_a , S_m , β_m , $\beta_a(r_0)$ need to be known in advance when applying the Fernald method to retrieve the aerosol optical properties. $\beta_a(r_0)$ is the aerosol backscatter coefficient at a height of r_0 .

3.1. Retrieving Aerosol Optical Properties with Mie-Scattering Lidar

During the joint measurements with CDL and Mie-scattering lidar, aerosol extinction coefficient at 532 nm α_a^{532} , and aerosol backscatter coefficient at 532 nm, β_a^{532} could be calculated from Mie-scattering lidar measurements using the Fernald method; in the calculation process, the aerosol lidar ratio $S_a^{532} = 50sr$ under the normal weather conditions. Normalized backscatter power of CDL can be obtained from the power spectra of CDL according to Appendix A, which is expressed as Equation (4):

$$\langle P_{1550nm,CDL}(R) \rangle = C[\beta_a^{1550}(R) + \beta_m^{1550}(R)] \exp[-2 \int_0^R \alpha_a^{1550}(r) + \alpha_m^{1550}(r) dr] \quad (4)$$

where $\langle P_{1550nm,CDL}(R) \rangle$ is the normalized backscatter power of CDL at height R , α_a^{1550} is the aerosol extinction coefficient at 1550 nm, β_a^{1550} is the aerosol backscatter coefficient at 1550 nm, β_m^{1550} and α_m^{1550} are, respectively, the molecules backscatter coefficient and extinction coefficient at 1550 nm, and they can be obtained from the standard atmospheric model of the United States of 1976 and the Rayleigh scattering theory.

To apply the Fernald method to retrieve aerosol optical properties from $\langle P_{1550nm,CDL}(R) \rangle$, CDL aerosol lidar ratio S_a^{1550} , and reference aerosol backscatter coefficient $\beta_a^{1550}(r_{0,CDL})$ at height $r_{0,CDL}$ must be known in advance as well. According to the Ångström exponent and empirical value that Müller et al. [26]. reported, the most appropriate $S_a^{1550} = 29.978sr$ was chosen in our calculation process depending on the weather conditions and geographical location. The assumed conversion factor k_{β_a} of aerosol backscatter coefficient from 532 to 1550 nm is applied to calculate $\beta_a^{1550}(r_{0,CDL})$, and the conversion relation is shown as:

$$\beta_a^{1550}(r_{0,CDL}) = \beta_a^{532}(r_{0,CDL}) k_{\beta_a} \quad (5)$$

An iterative retrieval method is proposed to determine k_{β_a} to obtain the final β_a^{1550} and α_a^{1550} , and specific calculation procedures are shown in Figure 1. Where i is the number of iterations, the coincident detection range of two lidars is from R_{\min} to R_{\max} , R_{\min} is the lowest detection altitude of Mie-scattering lidar, $R_{\max} = r_{0,CDL}$ is the highest detection altitude of CDL.

Firstly, $k_{\beta_a,0}$ is assumed as an arbitrary value other than zero, and the $\beta_a^{1550}(r_{0,CDL})$ could be calculated using the relationship of Equation (5). Then, $\beta_a^{1550}(R)$ could be retrieved by bringing $\beta_a^{1550}(r_{0,CDL})$ into Equation (4). Meanwhile the new conversion factor $k_{\beta_a,1}$

could be calculated according to the Equation (6) which means the ratio of the integral of β_a^{1550} to the integral of β_a^{532} in the coincident detection range.

$$k_{\beta_{a,i}} = \frac{\int_{500}^{2000} \beta_{a,i}^{1550}(r) dr}{\int_{500}^{2000} \beta_a^{532}(r) dr} \tag{6}$$

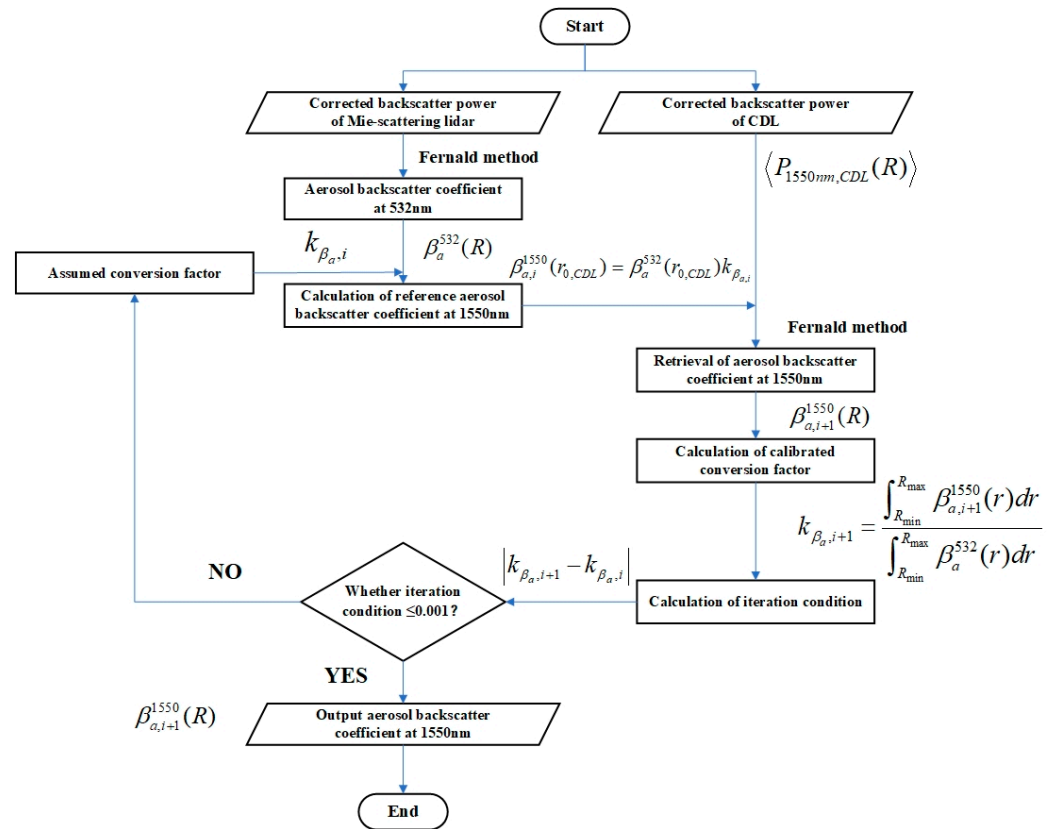


Figure 1. Overview of the iteration procedure.

Subsequently, the absolute value of subtraction between $k_{\beta_{a,1}}$ and $k_{\beta_{a,0}}$ is calculated. If the result is smaller than 0.001, the iteration process is stopped, and $\beta_{a,1}^{1550}(R)$ is the desired result. If not, the process mentioned above is repeated and the next iteration is operated to retrieve the new $\beta_{a,i}^{1550}(R)$.

Until the absolute value of subtraction between $k_{\beta_{a,i+1}}^{532 \rightarrow 1550}$ and $k_{\beta_{a,i}}^{532 \rightarrow 1550}$ satisfies the iteration criteria, this iterative process is stopped and $\beta_{a,i+1}^{1550}(R)$ is desired. The final aerosol extinction coefficient $\alpha_{a,i+1}^{1550}(R)$ could be obtained as well, depending on the lidar ratio of CDL. It takes about 3–5 iterations to get reliable results

3.2. Retrieving Aerosol Optical Properties with Atmospheric Visibility

Due to the limitation of the CDL measurement range, the altitude of the lowest retrieved backscatter power is 100 m. The estimated $\alpha_{near-ground}^{1550}$ cannot be directly used as a reference to retrieve aerosol optical properties. A near-surface linear conversion factor k_α between $\alpha_{near-ground}^{1550}$ and the aerosol extinction coefficient at an altitude of 100 m α_{100m}^{1550} could be obtained to solve this problem. Through multiple joint experiments, the conversion factor could be acquired by Equation (7). Then, the reliable k_α is also determined by averaging the daily averaged conversion factor.

$$k_\alpha = \frac{\alpha_{100m}^{1550}}{\alpha_{near-ground}^{1550}} \quad (7)$$

where α_{100m}^{1550} is retrieved from the first method and $\alpha_{near-ground}^{1550}$ is estimated by visibility.

After substituting corrected α_{100m}^{1550} and S_a^{1550} into Equation (4), the aerosol backscatter coefficient $\beta_{a,visibility}^{1550}$ and extinction coefficient $\alpha_{a,visibility}^{1550}$ of CDL could be retrieved by using the forward integral Fernald method in the subsequent joint measurements.

4. Experimental Results and Discussion

4.1. Experiment Information

Joint measurements among the sun photometer of the Beijing_CAMS site, CDL, and Mie-scattering lidar were specially designed and operated to complete the verification of these two proposed methods. The datasets of 29-day experiments from 1 September 2021 to 14 December 2021 were applied to validate the retrieval method with Mie-scattering lidar, which were also regarded as calibration datasets to determine the reliable k_α of the visibility-related retrieval method. Seven-day experimental datasets from 16 December 2021 to 31 December 2021 were used to verify the feasibility of the retrieval method with atmospheric visibility. Moreover, the corresponding daily AERONET datasets and real-time visibility datasets were calculated to obtain the reference $AE_{reference}^{532-1550}$ and corrected α_{100m}^{1550} . The experimental arrangements including retrieval methods, date, and purpose are introduced in Table 3.

Table 3. Experimental arrangements of two retrieval methods.

Retrieval Method	Date	Purpose
With Mie-scattering aerosol lidar	September 1st to December 14th	Retrieval and validation
With atmospheric visibility	September 1st to December 14th December 16th to December 31st	Calibration of reliable k_α Retrieval and validation

It should be noted that, as a polarization-sensitive lidar system with coupling and heterodyne processes, CDL only measures the backscatter light component with the same polarization direction as the LO light. Resulting from the effect of aerosol particle sphericity, backscatter light consists of horizontally polarized and vertically polarized light. Thus, the above methods should be used with caution for special weather conditions, e.g., dust and volcanic ash aerosols with depolarization ratios larger than 0.1 at 532 nm. Furthermore, to confirm the reliability of the inversion results, R_a is the proportion of aerosol content in the coincident detection range (from R_{min} to R_{max}), which must be higher than or equal to 80% of the total in the Mie-scattering lidar detection range. The calculation formula is written as:

$$R_a = \frac{\int_{R_{min}}^{R_{max}} P_{Mie}(r) dr}{\int_{500}^{10000} P_{Mie}(r) dr} \times 100\% \quad (8)$$

where P_{Mie} is the normalized backscatter power of Mie-scattering lidar, R_{max} is the altitude corresponding to the minimum signal-to-noise ratio (SNR) threshold of this CDL detection, SNR is equal to -30 dB [27].

It is emphasized that all the experimental datasets on the dusty days or the days whose R_a is less than 80% were respectively removed with the help of the “dust score index” data provided by AIRS/Aqua [28] and Equation (8). The experimental periods of each day are not the same, because of the influences of weather changes and device performance. The specific results and discussion will be reported in the next subsection.

4.2. Retrieval of Aerosol Optical Properties with Mie-Scattering Lidar

Synchronizing the operating time among CDL, Mie-scattering aerosol lidar, and sun-photometer of Beijing_CAMS site, 29-day experiments were performed under the filter

weather conditions for verifying the practicality of this retrieval method. The detailed calculation procedure is shown in Figure 2. To validate the retrieved aerosol optical properties, Ångström exponents (calculated by α_a^{1550} and α_a^{532}) of these two lidars $AE^{532-1550}$ were compared with $AE_{reference}^{532-1550}$. Three-day experiment results (including October 20th, November 17th, and December 14th) with representativeness are selected and separately shown in Figure 3a–c. The excellent temporal continuity between $AE^{532-1550}$ (black dots) and $AE_{reference}^{532-1550}$ (red dots) can be found in these figures, even if there are several outliers. These outliers are most likely due to the brief presence of dust mass or clouds above the boundary layer, which affected detection consistency between CDL and the sun-photometer.

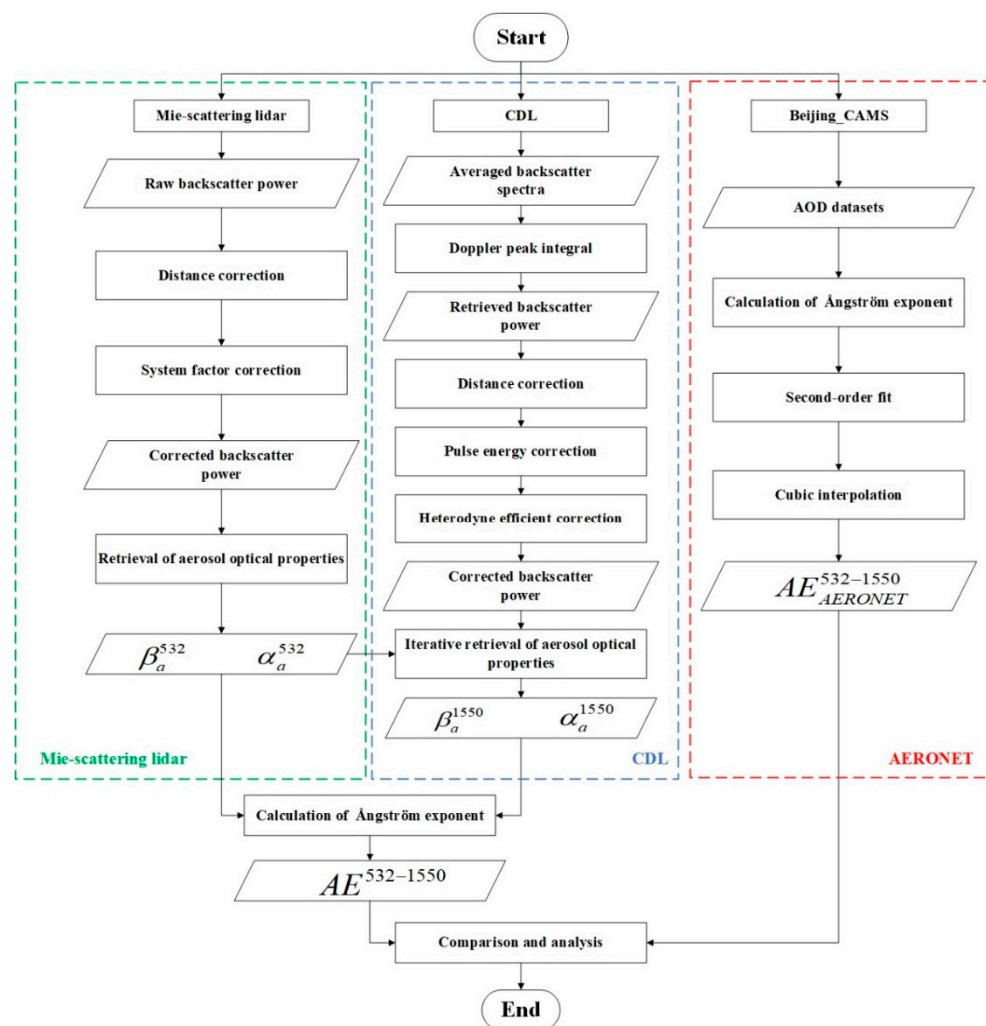


Figure 2. The flowchart shows the retrieval and verification procedures of aerosol optical properties with Mie-scattering aerosol lidar.

To further confirm the correctness of the retrieval method, cubic interpolation was applied to the datasets of $AE_{reference}^{532-1550}$ for calculating the time-synchronized Ångström exponent $AE_{AERONET}^{532-1550}$ with $AE^{532-1550}$. Moreover, the Grubbs test [29,30] was introduced as data quality control for rejecting outliers in this paper, and the confidence interval was set to 90%. Making a comparison between filtered $AE^{532-1550}$ and standard $AE_{AERONET}^{532-1550}$ to verify the correctness of obtained aerosol optical properties, all corresponding results are presented in Figure 4. In this figure, the x-axis represents filtered $AE^{532-1550}$, the y-axis represents $AE_{AERONET}^{532-1550}$, black dots are the filtered real-time corresponding relations of these two Ångström exponents, and the red line is obtained by linear fitting of these black dots. It is emphasized that the blue dots are the ones removed by the Grubbs test. Additionally,

evaluation indicators of this retrieval method are listed in the embedded table, from which the slope of the fitting line is 0.9779, the data number is 399, the root-mean-square error (RMSE) is 0.0342, the correlation coefficient R^2 is 0.93064, and the mean relative error is 0.0272. These verification results indicate the excellent performance of the retrieval method with Mie-scattering aerosol lidar.

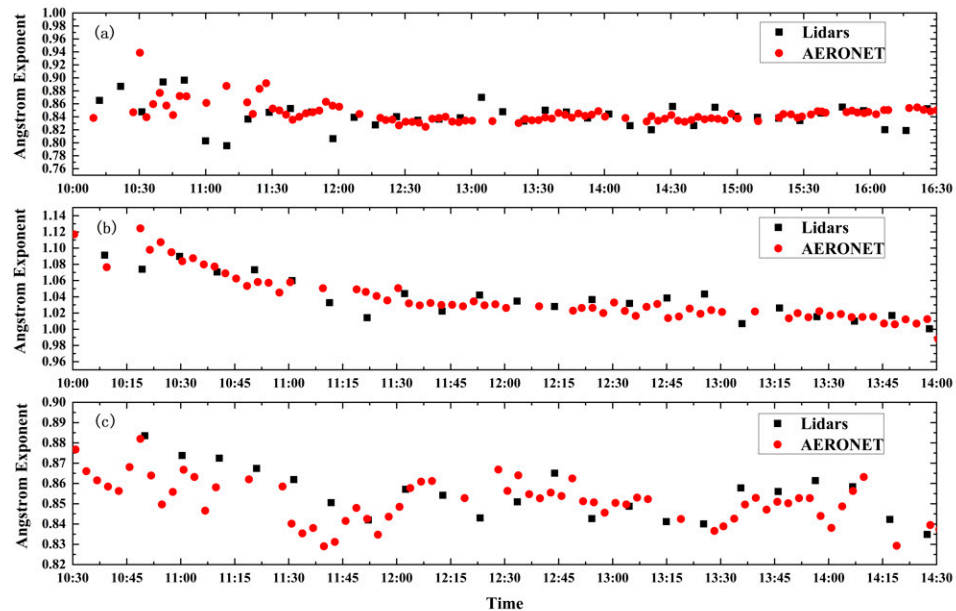


Figure 3. Ångström exponents comparison of three-day experiment, where $AE^{532-1550}$ (black dots) with 10 min temporal resolution are retrieved from the datasets of joint measurements and $AE_{reference}^{532-1550}$ (red dots) with 5 min temporal resolution are retrieved from datasets of the AERONET site. (a) 20 October 2021, (b) 17 November 2021, and (c) 14 December 2021.

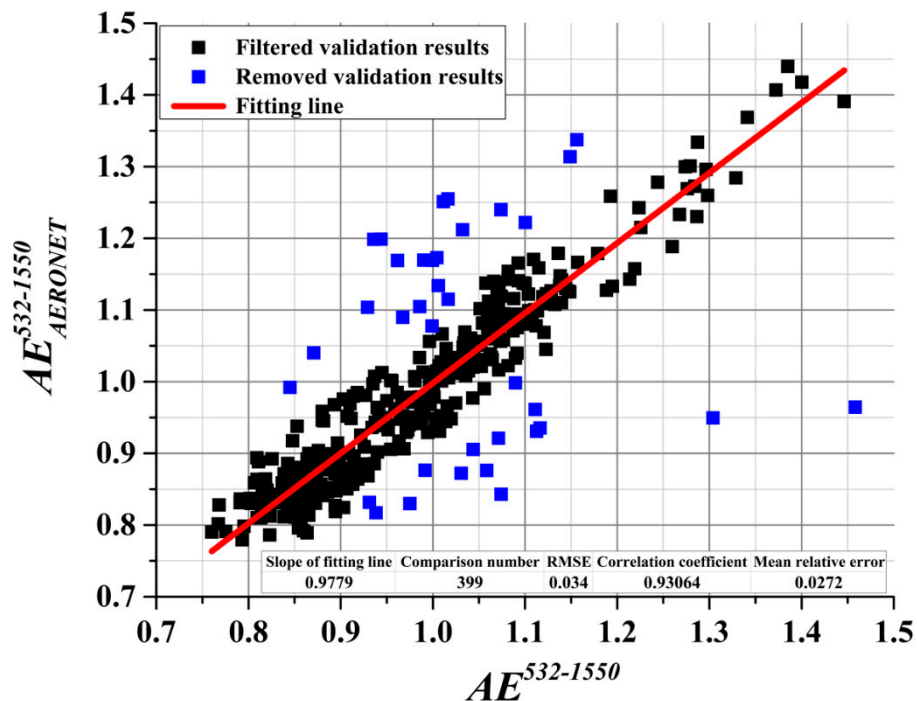


Figure 4. Validation results of all joint measurements for the retrieval method with Mie-scattering lidar. The black dots are the filtered relationship of $AE^{532-1550}$ and $AE_{AERONET}^{532-1550}$, the blue dots are the removed ones, the red line is obtained by linear fitting of verification results, the embedded table shows the detailed evaluation indicators of this retrieval method.

Lidar ratio deeply affects the inversion results, especially for this retrieval method, because the lidar ratios of these two lidars are both empirical values. To obtain the relationship between the retrieved aerosol optical properties and the lidar ratios, a representative dataset of October 20 is selected to indicate this relationship. Figure 5a shows that the retrieved β_a^{1550} varies with the change in S_a^{532} , when $S_a^{1550} = 29.978sr$. In this figure, the retrieved β_a^{1550} becomes smaller as the input S_a^{532} decreases. Correspondingly, Figure 5b shows that the retrieved β_a^{1550} varies with the change in S_a^{1550} , when $S_a^{532} = 50sr$. From this figure, we can find that the retrieved β_a^{1550} gets smaller as the S_a^{1550} increases.

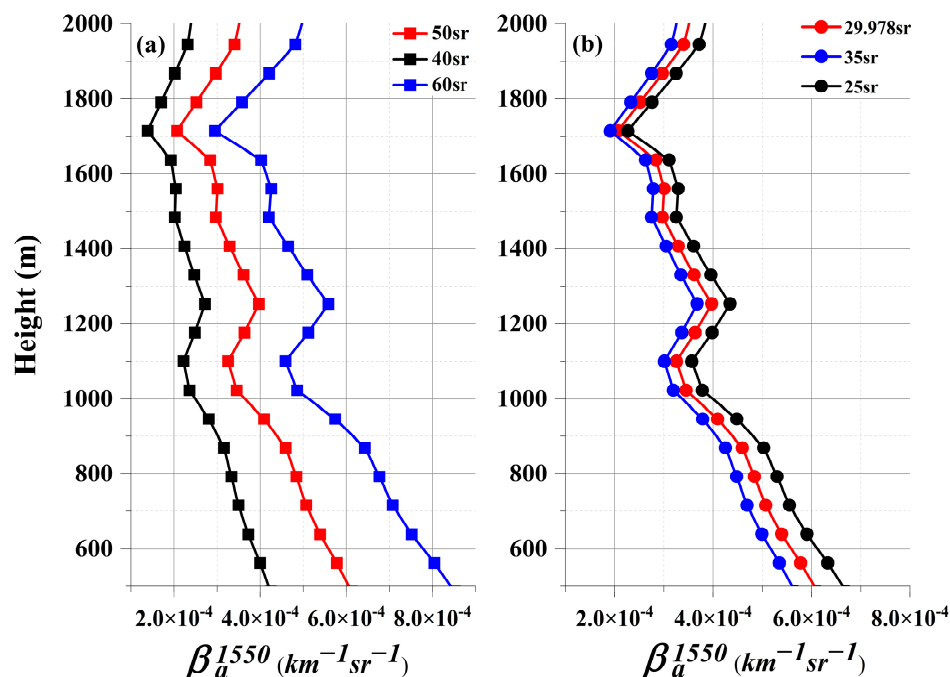


Figure 5. Relationship between lidar ratios and the retrieved aerosol backscatter coefficients. (a) When $S_a^{1550} = 29.978sr$, the retrieved β_a^{1550} changes with different S_a^{532} s input. (b) When $S_a^{532} = 50sr$, the retrieved β_a^{1550} changes with different S_a^{1550} s input.

Lastly, a typical weather process case on 23 November 2021 is chosen to better describe the aerosol distribution and transport process. The temporal and spatial variations in β_a^{532} , β_a^{1550} , and vertical wind speed are separately shown in Figure 6a–c. Strong, positive vertical wind speed appears at a low altitude between 11:00 and 12:15, then the height of the boundary layer increases significantly between 11:15 and 14:00. Comparatively, the height of the boundary layer gradually decreases after 15:00, because of the appearance of strong, negative vertical wind speed at around a height of 1000 m between 14:45 and 15:45. This phenomenon reveals that vertical wind speed can affect the distribution and diffusion of aerosol particles in the altitude range. At the same time, these experimental results confirm the feasibility and accuracy of CDL measuring the aerosol optical properties.

4.3. The Retrieval Method with Atmospheric Visibility

Based on the verification results of the retrieval method with Mie-scattering lidar, we proposed a more practical retrieval method with atmospheric visibility to calculate aerosol optical properties. The detailed procedures are presented in Figure 7. Filtered datasets of 29-day experiments from 1 September 2021 to 14 December 2021 were used to define the key factor k_α , which is shown in Figure 8. The reliable k_α can be calculated through the daily averaged conversion factors (red solid dots), the value is approximately equal to 0.2165.

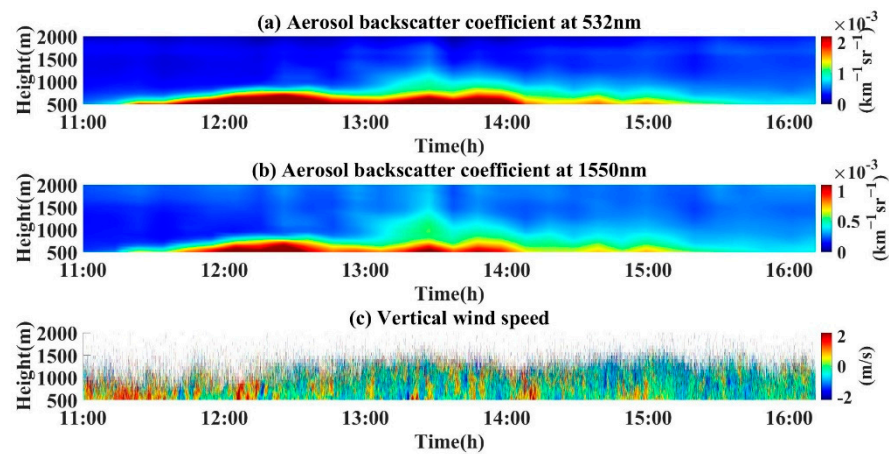


Figure 6. The time–space diagram of joint measurements results on 23 November 2021. (a) Aerosol backscatter coefficient at 532 nm in 10 min and 2.5 m resolution of Mie-scattering aerosol lidar, (b) aerosol backscatter coefficient at 1550 nm in 10 min and 60 m resolution of CDL, and (c) vertical wind speed in 1 s and 60 m resolution of CDL.

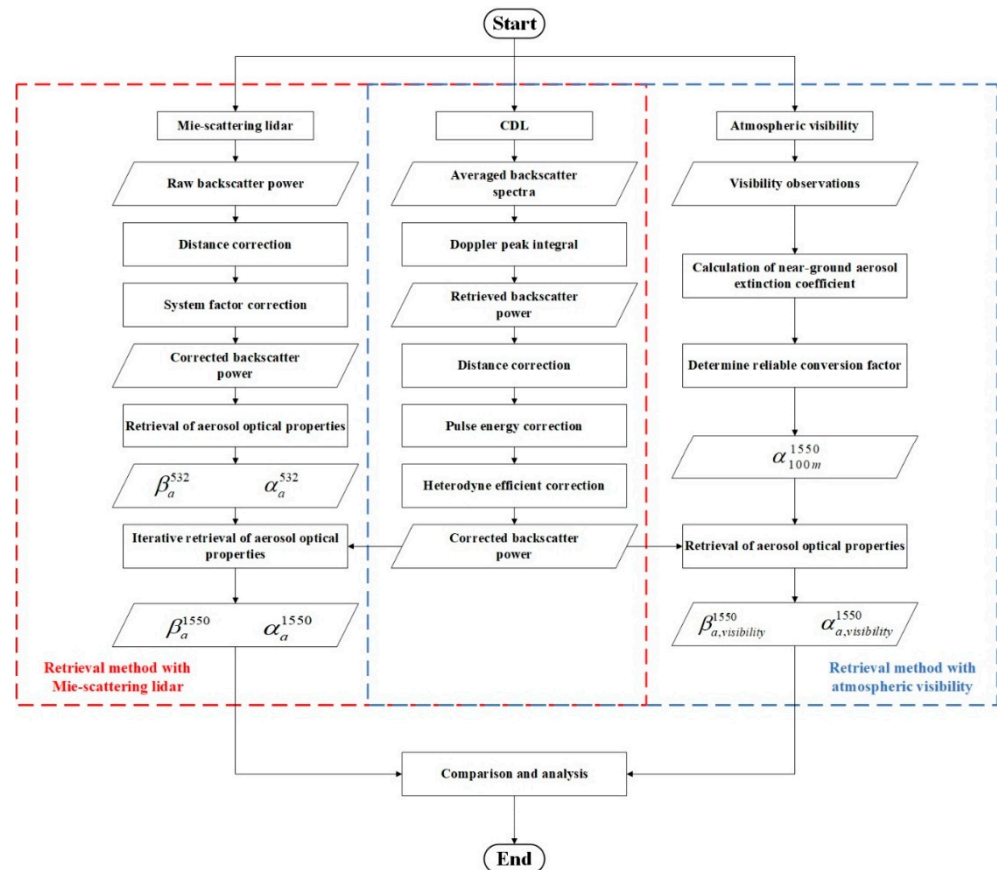


Figure 7. The flowchart shows the retrieval and verification procedures of aerosol optical properties with atmospheric visibility.

By the application of reliable k_α in the subsequent verification experiments, the aerosol optical properties of CDL could be calculated. The datasets of seven-day experiments from 16 December 2021 to 31 December 2021 were used to verify the feasibility of this visibility-related method. The corresponding results of all seven-day datasets are shown in Figure 9, where the x-axis represents β_a^{1550} which was calculated through the retrieval method with Mie-scattering lidar, and the y-axis represents $\beta_{a,visibility}^{1550}$ which was calculated

through the retrieval method with atmospheric visibility. In addition, the corresponding relationship (blue dots) between β_a^{1550} and $\beta_{a,visibility}^{1550}$, the fitting line (red line), and the detailed evaluation results (embedded table) are also demonstrated in this figure. From the embedded table, significant parameters could be obtained, including the slope of the fitting line is 0.9167, the data number is 2700, the coefficient of correlation R^2 is 0.9179, the root-mean-square error (RMSE) is 2.0619×10^{-4} , and the mean relative error is 0.1423. Since the standard β_a^{1550} was retrieved with Mie-scattering lidar, two mean relative errors of these retrieval methods should be considered as the accuracy one for this visibility-related method. The final mean relative error of this method is only 0.1656.

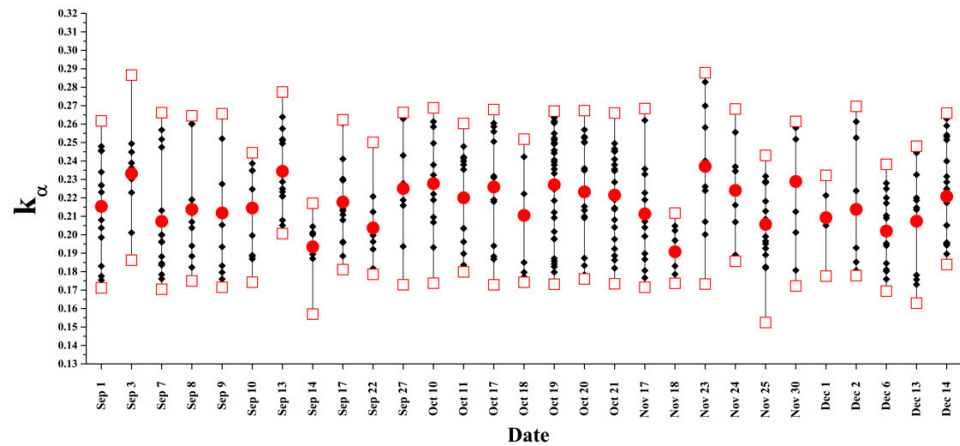


Figure 8. Statistical chart of daily conversion factors. The black dots are the conversion factors in each day, temporal resolution is 10 min, two hollow square dots located on the top and bottom are the maximum and minimum, respectively, for each day, and the red solid dots represent the mean conversion factor for each day.

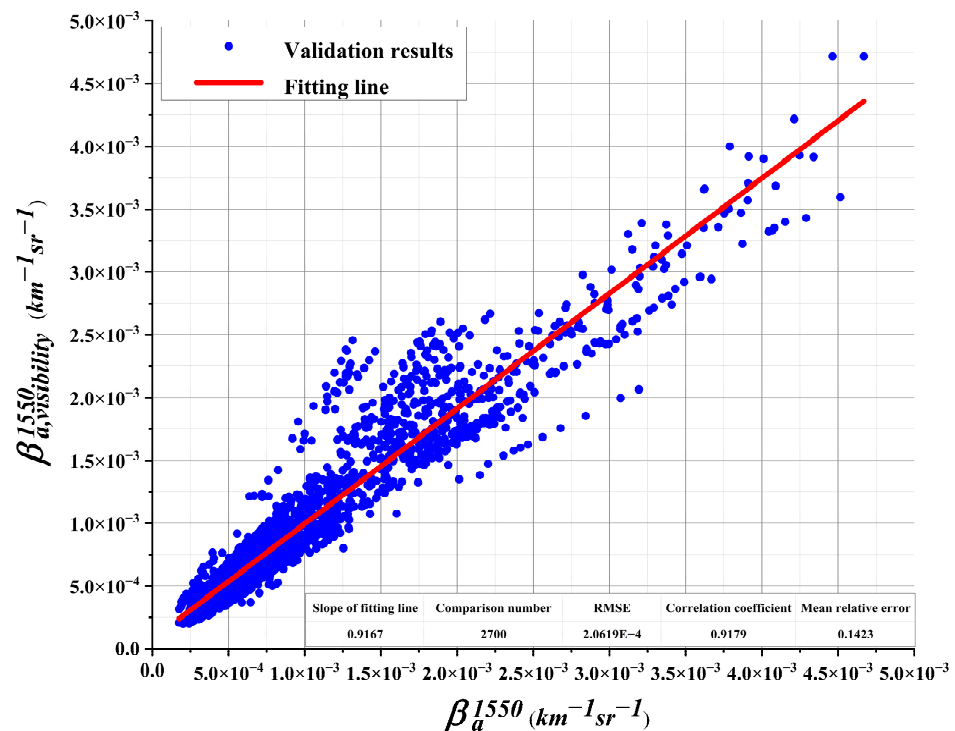


Figure 9. Validation results of all joint measurements for retrieval method with atmospheric visibility. The blue dots are the relationship of β_a^{1550} and $\beta_{a,visibility}^{1550}$, the red line is obtained by linear fitting of validation results, the embedded table shows the detailed evaluation indicators of this retrieval method.

A joint measurement case on December 22nd is presented in Figure 10, where aerosol backscatter coefficients retrieved with Mie-scattering lidar and atmospheric visibility are respectively shown in Figure 10a,b; the vertical wind speed measured by CDL is shown in Figure 10c. From these figures, we can find that the spatial–temporal changes in the two backscatter coefficients have a great similarity, even though there is a slight difference around 21 o'clock and around 23 o'clock. The time resolution of visibility is 1 h greater than that of joint measurement, which is the main reason caused this difference. Furthermore, the vertical wind speed is small and has no obvious variation during the joint measurements period, which has no significant impact on aerosol distribution and transport. From Figure 10a,b, it also can be seen that the aerosol particles are mainly distributed below 1500 m, and the height of the boundary layer is almost unchanged.

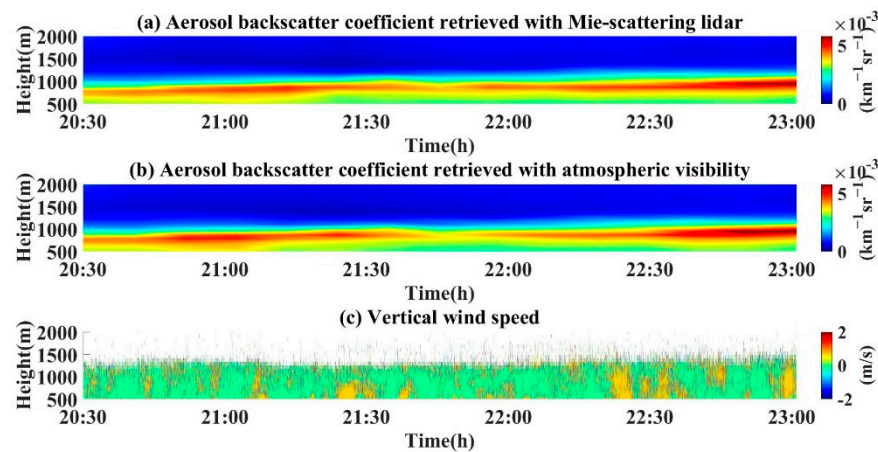


Figure 10. The time–space diagram of joint measurements results on 22 December 2021. (a) Aerosol backscatter coefficient at 1550 nm in 10 min and 60 m resolution of the retrieval method with Mie-scattering aerosol lidar, (b) aerosol backscatter coefficient at 1550 nm in 10 min and 60 m resolution of the retrieval method with atmospheric visibility, and (c) vertical wind speed in 1 s and 60 m resolution of CDL.

5. Conclusions

Two practical methods for retrieving aerosol optical properties with CDL were described in this paper which were based on the datasets of Mie-scattering lidar and atmospheric visibility, respectively. Experimental results demonstrate the feasibility of these two methods. The results and significant conclusions are summarized and discussed as follows.

For the retrieval method with Mie-scattering lidar, the reference value $\beta_a^{1550}(r_0)$ is determined by the assumed conversion factor k_{β_a} . Then, the iteration of k_{β_a} leads to the final β_a^{1550} and α_a^{1550} . To validate the retrieval results, $AE^{532-1550}$ was estimated from the datasets of obtained aerosol optical properties and respectively compared with $AE_{reference}^{532-1550}$ and $AE_{AERONET}^{532-1550}$ which were calculated from the datasets of the Beijing_CAMS site. A good temporal continuity (the slope of the fitting line is 0.9779, the data number is 399, RMSE is equal to 0.034, the correlation coefficient is 0.93064, and the mean relative error is 0.0272) could be obtained from the validation results.

After verifying the feasibility of the first retrieval method, a more functional method based on atmospheric visibility was proposed to retrieve aerosol optical properties. Through the visibility datasets and the results of the first method, α_{100m}^{1550} could be obtained to calculate aerosol optical properties. The subsequent joint measurements with CDL and Mie-scattering lidar, β_a^{1550} and $\beta_{a,visibility}^{1550}$ were retrieved using these two methods individually. The two backscatter coefficients were compared to validate the visibility-related method, which shows great agreement: the slope of the fitting line is 0.9167, the data number is 2700, RMSE is equal to 2.0619×10^{-4} , the correlation coefficient is 0.9179, and the mean relative error is 0.1423. Noteworthily, combining the verification process, the total mean relative error of this retrieval method is only 0.1656. These mean aerosol optical

properties retrieval based on CDL observation accurately becomes possible. However, it is still necessary to continue performing joint measurements to calibrate the reliable k_α , making the inversion results of this visibility-related retrieval method more convincing.

The above retrieval methods should be used with caution under the aerosol load with high depolarization ratio, and weather conditions such as dust and volcanic ash whose depolarization ratios are larger than 0.1 at 532 nm. It is emphasized that the limitation will no longer exist once we have completed the upgrade of the experimental CDL system, expanding CDL's ability to detect dual-polarization backscatter light. The subsequent calibration and verification experiments will be operated by joint measurements with CDL and other reference lidars. After system performance calibration, this CDL would be a breakthrough for these retrieval methods applied to all the aerosol loads.

In further studies, the validation measurements of CDL dual-polarized detection with other reference lidars will be prioritized, which will reduce aerosol particles' depolarization effects and obtain more accurate backscatter signals. In subsequent joint observations, aerosol optical properties and vector wind fields will be obtained in various weather conditions to demonstrate the temporal and spatial variation in aerosols in detail. Furthermore, improving the measurement height and range resolution of CDL, so that comprehensive aerosol transport and physical mechanisms would be measured by the aforementioned retrieval methods.

Author Contributions: Conceptualization, Y.Z. (Yinchao Zhang) and P.G.; methodology and writing, Y.Z. (Yize Zheng) and W.T.; joint measurements and dataset calculation, Y.Z. (Yize Zheng) and Q.X.; suggestions of theoretical calculations and method improvements, Y.Z. (Yinchao Zhang), W.T., P.G. and S.C. (Su Chen); CDL program upgrade, R.L.; project administration, Y.Z. (Yinchao Zhang), S.C. (Siyang Chen) and H.C.; validation, Y.Z. (Yize Zheng), S.C. (Su Chen) and Q.X. All authors have read and agreed to the published version of the manuscript.

Funding: This research was funded by the China Postdoctoral Science Foundation (2020M680369).

Data Availability Statement: Data can be accessed by contacting Wangshu Tan (tanws@bit.edu.cn).

Conflicts of Interest: The authors declare no conflict of interest.

Appendix A

The raw backscatter signal power retrieval processes from power spectra of CDL. For a single shot, backscatter light and local oscillator (LO) light are mixed by a coupler, then passed through a balanced detector with uniform responsivity for removing the common-mode signal. Retained heterodyne photocurrent can be written as [11]:

$$i_h(t) = \eta_q \frac{e}{h\nu} A_d \sqrt{\eta_h(t) P_{LO} P_S} \cos(2\pi\Delta f t + \Delta\varphi(t)) \quad (\text{A1})$$

where i_h is the output photocurrent from the balanced detector, t is the elapsed time since the pulse laser emitted, η_q is the quantum efficiency of the detector, e is the electron charge, h is the Planck constant, ν is the laser frequency, A_d is the photosensitive area of the balanced detector, η_h is the heterodyne efficiency reflecting the matching rate of phase and amplitude between the LO light and the backscatter light, P_{LO} is the LO light power at the detector plane, P_S is the received backscatter light power at the detector plane, Δf and $\Delta\varphi$ are, respectively, the frequency difference and the phase difference between backscatter light and LO light.

After analog-to-digital conversion (A/D) and fast Fourier transformation by an acquisition board, the heterodyne photocurrent is transformed into range-resolved power spectra. With the given range gate at distance R , the received backscatter signal within

the same range gate is supposed to be constant. The power spectra approximation is expressed as:

$$\hat{P}(R, k) = \frac{1}{N} \left(\frac{2\eta_{qe}}{h\nu} R_{in} G \right)^2 P_{LO} P_S(R) \bullet \left| \sum_{n=N_1}^{N_2} \sqrt{\eta_h(nT_s)} \cos(2\pi\Delta nT_s + \Delta\varphi(nT_s)) e^{-j\frac{2\pi kn}{N}} \right|^2 \quad (A2)$$

where N is the number of samples within a range gate, T_s is the sampling time, R_{in} is the input impedance of the acquisition board, G is the signal gain of devices, $N_1 = N_R - N/2$, $N_2 = N_R + N/2$, N_R is the sample point located at the center of the range gate and it is given by the integer part of $N_R = (2R/T_s c)$, c is the light speed. Due to the influence of the speckle effect [13] the power spectra of different pulse shots vary greatly. To reduce this influence and improve the signal-to-noise (SNR) as well, the power spectra of many shots are averaged as shown in Equation (A3).

$$\hat{P}(R, k)_{ave} = \frac{1}{I} \sum_{i=1}^I \hat{P}(R, k) \quad (A3)$$

The power spectrum $\hat{P}(R, k)$ of a range gate at distance R corresponds to shot i and I is the shot number for averaging. According to the acquisition parameters and device performance, when laser pulse repetition is 10 kHz and setting $I = 10,000$, the corresponding temporal resolution is 1 s.

The CDL is a pre-triggered acquisition system, the acquisition card collects a length of internally electronic noise which is equal to the length of each range gate before the laser pulse emits. Emphatically, the previous formula derivation has omitted the relevant noise effects, and the noise floor is subtracted during the calculation processing of averaged power spectra. In order to estimate backscatter power from power spectra, the corresponding power spectra components of the doppler peak within the range gate are summed. A generally practical estimator for calculating radial wind speed is named the center of gravity estimator, which is used in this paper to determine the width of the doppler peak. The left side of the peak is from spectral maximum to the first trend change point (K_1) on the left side and the same for the right side (K_2). The expected value of backscatter power is calculated by integrating the doppler peak within the corresponding range gate of averaged power spectra:

$$\langle P(R) \rangle = \sum_{k=K_1}^{K_2} \hat{P}(R, k)_{ave} = \frac{1}{N} \left(\frac{2\eta_{qe}}{h\nu} R_{in} G \right)^2 P_{LO} P_S(R) \eta_h(R) \quad (A4)$$

According to the lidar equation [2], the received backscatter power P_S of range gate at distance R could be written as:

$$P_S(R) = O(R) \eta_o \frac{A_R c}{R^2} \frac{c}{2} E_x \beta(R) T^2(R) \quad (A5)$$

where E_x is the laser pulse energy, β is the backscatter coefficient, $T(R) = \exp\left[-\int_0^R \alpha(r) dr\right]$ is the atmospheric transmission, A_R is the area of the telescope, is the extinction coefficient, η_o is the optical system loss, $O(R)$ is the overlap function which is regarded as 1 in this coaxially a-focal wind lidar system. Replacing Equation (A5) into Equation (A4) and combining all constants in one constant C , thus Equation (A4) can be rewritten as:

$$\langle P(R) \rangle = \frac{C}{R^2} E_x \eta_h(R) \beta(R) T^2(R) \quad (A6)$$

where $C = \frac{1}{N} \left(\frac{2\eta_{qe}}{h\nu} R_{in} G \right)^2 P_{LO} \eta_o A_R \frac{c}{2}$.

For the sake of obtaining a direct relationship among received backscatter power, backscatter coefficient, and transmittance, the backscatter power calculated by Equation (A6) requires correction, including range correction, pulse energy correction, and heterodyne efficiency correction. The corrected Equation (A6) is rewritten as:

$$\frac{\langle P(R) \rangle R^2}{E_x \eta_h(R)} = C \beta(R) T^2(R) \quad (\text{A7})$$

where the laser output pulse energy is modulated by current and temperature, it is monitored by the input pump current simultaneously. Because the effect of turbulence is complex, it is difficult to estimate turbulence with an exact formula. In the measurement conditions where aerosols are relatively stable, the turbulence effect could be neglected. Hence, neglecting the turbulence effect and assuming CDL is a monostatic a-focal untruncated Gaussian beam lidar. The heterodyne efficiency can be approximated with the following expression [11]:

$$\eta_h(R) = \left[1 + \left(\frac{\pi \rho^2}{\lambda R} \right)^2 \right]^{-1} \quad (\text{A8})$$

where ρ is the e^{-2} irradiance beam radius and λ the laser wavelength. However, the heterodyne efficiency shown in (A8) is not suitable for all measurement conditions. To ensure the accuracy of corrected backscatter power, the reliable heterodyne efficiency function is obtained by polynomial fitting to the normalized backscatter power [13].

System constant C is difficult to obtain directly according to the known lidar parameters. The whole calculation processes of the two retrieval methods introduced in Section 3 exclude using the system constant C .

References

- Boucher, O.; Randall, D.; Artaxo, P.; Bretherton, C.; Feingold, G.; Forster, P.; Kerminen, V.-M.; Kondo, Y.; Liao, H.; Lohmann, U.; et al. Clouds and Aerosols. In *Climate Change 2013: The Physical Science Basis. Contribution of Working Group I to the Fifth Assessment Report of the Intergovernmental Panel on Climate Change*; Cambridge University Press: Cambridge, UK, 2013; pp. 571–892; ISBN 978-1-107-66182-0.
- Milonni, D.P.W. Lidar. Range-Resolved Optical Remote Sensing of the Atmosphere, in the Springer Series in Optical Sciences, Vol. 102, Edited by Claus Weitkamp. *Contemp. Phys.* **2009**, *50*, 601–602. [[CrossRef](#)]
- Wandinger, U.; Linne, H.; Bosenberg, J. Turbulent aerosol fluxes determined from combined observations with doppler wind and raman aerosol lidar. In *Proceedings of the 22nd International Laser Radar Conference, Matera, Italy, 12–16 July 2004*; Volume 561, p. 743.
- Bou Karam, D.; Flamant, C.; Knippertz, P.; Reitebuch, O.; Pelon, J.; Chong, M.; Dabas, A. Dust Emissions over the Sahel Associated with the West African Monsoon Intertropical Discontinuity Region: A Representative Case-Study. *Q. J. R. Meteorol. Soc.* **2008**, *134*, 621–634. [[CrossRef](#)]
- Schumann, U.; Weinzierl, B.; Reitebuch, O.; Schlager, H.; Minikin, A.; Forster, C.; Baumann, R.; Sailer, T.; Graf, K.; Mannstein, H.; et al. Airborne Observations of the Eyjafjalla Volcano Ash Cloud over Europe during Air Space Closure in April and May 2010. *Atmos. Chem. Phys.* **2011**, *11*, 2245–2279. [[CrossRef](#)]
- Weinzierl, B.; Sauer, D.; Minikin, A.; Reitebuch, O.; Dahlkötter, F.; Mayer, B.; Emde, C.; Tegen, I.; Gasteiger, J.; Petzold, A.; et al. On the Visibility of Airborne Volcanic Ash and Mineral Dust from the Pilot's Perspective in Flight. *Phys. Chem. Earth Parts ABC* **2012**, *45*, 87–102. [[CrossRef](#)]
- Bufton, J.L.; Hoge, F.E.; Swift, R.N. Airborne Measurements of Laser Backscatter from the Ocean Surface. *Appl. Opt.* **1983**, *22*, 2603. [[CrossRef](#)]
- Menzies, R.T.; Tratt, D.M. Airborne CO₂ Coherent Lidar for Measurements of Atmospheric Aerosol and Cloud Backscatter. *Appl. Opt.* **1994**, *33*, 5698. [[CrossRef](#)]
- Klett, J. Lidar Inversion with Variable Backscatter/Extinction Ratios. *Appl. Opt.* **1985**, *24*, 1638–1643. [[CrossRef](#)] [[PubMed](#)]
- Böckmann, C.; Wandinger, U.; Ansmann, A.; Bösenberg, J.; Amiridis, V.; Boselli, A.; Delaval, A.; Tomasi, F.D.; Frioud, M.; Grigorov, I.V.; et al. Aerosol Lidar Intercomparison in the Framework of the EARLINET Project. 2. Aerosol Backscatter Algorithms. *Appl. Opt.* **2004**, *43*, 977–989. [[CrossRef](#)] [[PubMed](#)]
- Henderson, S.W.; Gatt, P.; Rees, D.; Huffaker, R.M. Wind Lidar. In *Laser Remote Sensing*; CRC Press: Boca Raton, FL, USA, 2005; pp. 487–740; ISBN 0-429-13574-2.
- Engelmann, R.; Wandinger, U.; Ansmann, A.; Müller, D.; Žeromskis, E.; Althausen, D.; Wehner, B. Lidar Observations of the Vertical Aerosol Flux in the Planetary Boundary Layer. *J. Atmos. Ocean. Technol.* **2008**, *25*, 1296–1306. [[CrossRef](#)]

13. Chouza, F.; Reitebuch, O.; Groß, S.; Rahm, S.; Freudenthaler, V.; Toledano, C.; Weinzierl, B. Retrieval of Aerosol Backscatter and Extinction from Airborne Coherent Doppler Wind Lidar Measurements. *Atmos. Meas. Tech.* **2015**, *8*, 2909–2926. [[CrossRef](#)]
14. Dai, G.; Wang, X.; Sun, K.; Wu, S.; Song, X.; Li, R.; Yin, J.; Wang, X. Calibration and Retrieval of Aerosol Optical Properties Measured with Coherent Doppler Lidar. *J. Atmos. Ocean. Technol.* **2021**, *38*, 1035–1045. [[CrossRef](#)]
15. Rui, X.; Guo, P.; Chen, H.; Chen, S.; Zhang, Y.; Zhao, M.; Wu, Y.; Zhao, P. Portable Coherent Doppler Light Detection and Ranging for Boundary-Layer Wind Sensing. *Opt. Eng.* **2019**, *58*, 034105. [[CrossRef](#)]
16. Chen, H.; Chen, S.; Zhang, Y.; Chen, H.; Guo, P.; Chen, B. Experimental Determination of Raman Lidar Geometric Form Factor Combining Raman and Elastic Return. *Opt. Commun.* **2014**, *332*, 296–300. [[CrossRef](#)]
17. Ji, H.; Zhang, Y.; Chen, S.; Chen, H.; Guo, P. Aerosol Characteristics Inversion Based on the Improved Lidar Ratio Profile with the Ground-Based Rotational Raman–Mie Lidar. *Opt. Commun.* **2018**, *416*, 54–60. [[CrossRef](#)]
18. Holben, B.N.; Eck, T.F.; Slutsker, I.A.; Tanre, D.; Buis, J.; Setzer, A.; Vermote, E.; Reagan, J.A.; Kaufman, Y.; Nakajima, T. AERONET—A Federated Instrument Network and Data Archive for Aerosol Characterization. *Remote Sens. Environ.* **1998**, *66*, 1–16. [[CrossRef](#)]
19. King, M.D.; Byrne, D.M. A Method for Inferring Total Ozone Content from the Spectral Variation of Total Optical Depth Obtained with a Solar Radiometer. *J. Atmos. Sci.* **1976**, *33*, 2242–2251. [[CrossRef](#)]
20. Eck, T.F.; Holben, B.; Reid, J.; Dubovik, O.; Smirnov, A.; O’neill, N.; Slutsker, I.; Kinne, S. Wavelength Dependence of the Optical Depth of Biomass Burning, Urban, and Desert Dust Aerosols. *J. Geophys. Res. Atmos.* **1999**, *104*, 31333–31349. [[CrossRef](#)]
21. Nebuloni, R. Empirical Relationships between Extinction Coefficient and Visibility in Fog. *Appl. Opt.* **2005**, *44*, 3795. [[CrossRef](#)]
22. China Central Meteorological Observatory. Available online: <http://www.nmc.cn/publish/sea/seaplatform1.html> (accessed on 31 December 2021).
23. Löhle, F. Über Die Lichtzerstreuung Im Nebel. *Phys. Zeits* **1944**, *45*, 199–205.
24. Middleton, W.E.K. Vision through the Atmosphere. In *Vision Through the Atmosphere*; University of Toronto Press: Toronto, ON, Canada, 2019; ISBN 1-4875-8614-0.
25. Fernald, F.G. Analysis of Atmospheric Lidar Observations: Some Comments. *Appl Opt.* **1984**, *23*, 652–653. [[CrossRef](#)]
26. Müller, D.; Ansmann, A.; Mattis, I.; Tesche, M.; Wandinger, U.; Althausen, D.; Pisani, G. Aerosol-Type-Dependent Lidar Ratios Observed with Raman Lidar. *J. Geophys. Res.* **2007**, *112*, D16202. [[CrossRef](#)]
27. Lin, R.; Guo, P.; Chen, H.; Chen, S.; Zhang, Y. Smoothed Accumulated Spectra Based WDSWF Method for Real-Time Wind Vector Estimation of Pulsed Coherent Doppler Lidar. *Opt. Express* **2022**, *30*, 180. [[CrossRef](#)] [[PubMed](#)]
28. Earth Data. Available online: <https://earthdata.nasa.gov/earth-observation-data/near-real-time/hazards-and-disasters/dust-storms> (accessed on 31 December 2021).
29. Grubbs, F.E. Procedures for Detecting Outlying Observations in Samples. *Technometrics* **1969**, *11*, 1–21. [[CrossRef](#)]
30. Stefansky, W. Rejecting Outliers in Factorial Designs. *Technometrics* **1972**, *14*, 469–479. [[CrossRef](#)]